Magma pressure drop as a forecasting tool for the end of the 2021 La Palma eruption (Canary Islands)

M. Charco[1,*], P. J. González[2,*], L. García-Cañada[3] , J.L.G. Pallero[4] and C. del Fresno[3]

[1]Instituto de Geociencias (IGEO, CSIC-UCM), C/ Dr Severo Ochoa, 7, 28040 Madrid (Spain).

[2]Volcanology Research Group. Department of Life and Earth Sciences, Instituto de Productos Naturales y Agrobiología, Consejo Superior de Investigaciones Científicas (IPNA-CSIC), La Laguna, Canary Islands, Spain.

[3]Instituto Geográfico Nacional (IGN), Madrid, Spain

[4]ETSI en Topografía, Geodesia y Cartografía, Universidad Politécnica de Madrid, Madrid, Spain.

[*]Authors contributed equally

Corresponding author: María Charco (m.charco@csic.es); Pablo J. González (pabloj.gonzalez@csic.es)

Key Points:

- Eruption end forecast was uncertain but possible using ground deformation measurements.
- Hindcast improved analysis of the eruption end indicates bounds on practical applicability of such forecasts.
- Real-time ground deformation interpretation could represent a simple and powerful tool for volcano monitoring.

Abstract (150 palabras)

Accurate forecasting eruptive activity is a core challenge in volcanology. Here, we describe an end of eruption forecast during the 2021 La Palma eruption using continuous GNSS geodetic data. We observed that co-eruptive deflation resembled a quasi-exponential trend and used it to forecast when deflation would cease equating to when the eruption would end. The forecast was done within the eruption, however was not operational due to large uncertainty in the unknown pressure drop threshold needed to stop magma upflow. In hindcast, we explore minimum datasets needed and how forecast uncertainty reduces with increase in ingested data. We conclude that forecasts could be possible after the time-scale around the e-folding time of the exponential decay and quite accurate ones after twice that time-scale. Our results also indicate that the eruption was controlled by the dynamics of a Moho depth reservoir beneath Cumbre Vieja volcano.

Plain Language Summary

The forecast, an actual prediction of the temporal or spatial characteristics of a future event, of when a volcanic eruption will end is challenging. We were able to make such a forecast during an eruption using GNSS geodetic data that help track the changes in Earth's surface deformation. We exploited a temporal decaying deflating deformation pattern that could be interpreted as when the eruption would stop. We made this forecast 42 days before the eruption ended, although the forecast time window was too uncertain due to the unknown pressure needed to stop the magma to have practical application. With the eruption already over, we looked back at the data and found that the more information we could have analyzed, the more accurate their forecast could have been. We conclude that accurate forecasts could be possible after a characteristic time of the decay process has passed. Hence, we concluded that the volcano's activity was controlled by a reservoir deep (10-14 km) beneath the surface.

1 Introduction

Much attention is focused on forecasting the onset of eruptions by the interpretation of on-going short-term unrest (e.g., Sparks, 2003; Pallister and McNutt, 2015) or using the statistical analysis of the long-term record of repose periods (e.g., Marzocchi and Bebbington, 2012). Nevertheless, accurately forecasting the style, size and duration of eruptions is as important as understanding the mechanism by which volcanic eruptions are initiated and helps to support evacuation strategies around volcanic areas. Particularly important for preventing casualties during eruptions at which lava flows are one of its primary hazards is forecasting when an eruption will end. Place attachment, protecting assets or poor shelter conditions during the eruption can push evacuees to move back to their homes during high-risk periods.

Considerable efforts are made on relating changes in recorded unrest signals with specific subsurface processes (e.g., Segall, 2013; National Academies of Sciences, Engineering and Medicine, 2017; Poland and Anderson, 2019). Quasi-exponential trends on deformation have been observed at several volcanoes in different periods of unrest (e.g., Biggs and Pritchard, 2017; Rodríguez-Molina et al., 2021). During eruptions, there is observational evidence that effusion rates and/or volume change of some volcanoes decrease exponentially. In such a way, many effusive eruptions are characterized by effusion rates that exponentially decay with time (e.g., Machado, 1974; Wadge, 1981; Gudmundsson et al., 2016; Coppola et al., 2017). Furthermore, in many basaltic-effusive eruptions, the temporal evolution of ground deformation (e.g., tilt, vertical and horizontal displacement or volume of dome grow) follows quasi-exponential trends (e.g., Dvorak and Okamura, 1987; Stasiuk et al., 1993; Lengliné et al., 2008; Mastin et al., 2009; Hreinsdottir et al., 2014; Gudmundsson et al., 2016; Coppola et al., 2017) of the form:

$$s(t) = s_o\left(1 - e^{-t/\tau}\right) \quad (1)$$

where $s(t)$ is the change in the measured deformation quantity since $t = 0$, s_o is the constant value at which $s(t)$ tends when $t \to \infty$, and τ is the characteristic e-folding time. Such trends can be reasonably ascribed to elastic relaxation of a deep magma chamber and are well explained by physics based models that couple magma flow with reservoir pressurization (see e.g., Mastin et al., 2009; Anderson and Segall, 2011; Segall, 2013).

During the 2021 Cumbre Vieja volcanic eruption, a long-lasting (September 19 - December 13, 85 days of duration), hybrid eruption with alternation, or, more often, contemporaneous emission of lava flows and tephra, continuous GNSS geodetic data were recorded at eight permanent stations well spread around La Palma island (Figure 1 and S1). These geodetic data constitute a great example of regional syn-eruptive deflation (Figures 1 and 2) with a gradually decreasing rate. In this work, we show that this deflation significantly resembles the trend described by equation (1). During the eruption, this approach allowed us to theoretically forecast time at which deflation ceases assuming a close magma system in an elastic media. Therefore, we obtained a forecast of the end of the eruption by November, 1st 2021 - 42 days before the end of the eruption. Due to the large amount of uncertainty on the estimations this forecast was not relevant in operational terms.

In this work, we describe the methodology followed to provide an appropriate forecast. We noted that the uncertainties on data, on the extrapolation of the fitted trend as well as on the time-dependence modeling of the measured quantity result in relatively low practical uncertainty bounds on the exact forecasted eruption duration. In hindsight, with the eruption already ended, we analyzed the methodology for making such forecasts and derived some constraints about the magma system. We discuss the minimum dataset needed to make credible forecasts, as well as how prediction uncertainty diminishes with real time increase of data.

2 Data

La Palma Island has a well distributed continuously operating GNSS network formed by eight stations (Figures 1 and S1). The Instituto Geográfico Nacional (here and after IGN) installed LPAL, the first station on the island, in 2001. In 2010 Grafcan (Cartografica de Canarias S.A.) set up MAZO station. Finally, from 2015 to 2019 IGN developed a densification network for volcano monitoring formed by the other stations (LP01-LP06). We use 30-second sampling data to produce daily coordinate time series in the International Terrestrial Reference Frame 2014 (ITRF2014) (Altamimi et al., 2016), by applying a double-difference regional network strategy using the Bernese GPS software version 5.2 (Dach et al., 2015). The regional network is formed by more than 30 stations located in the Canary Islands and surrounding areas (Azores, south of Spain and north of Africa). Ocean-loading model FES2004 (Lyard et al., 2006), the IGS (International GNSS Service) absolute antenna phase center models and satellite orbits (Kouba, 2009) are used in the computation. In order to align to the ITRF2014 minimum constraints to an International GNSS Service (IGS) core site group of five stations are applied.

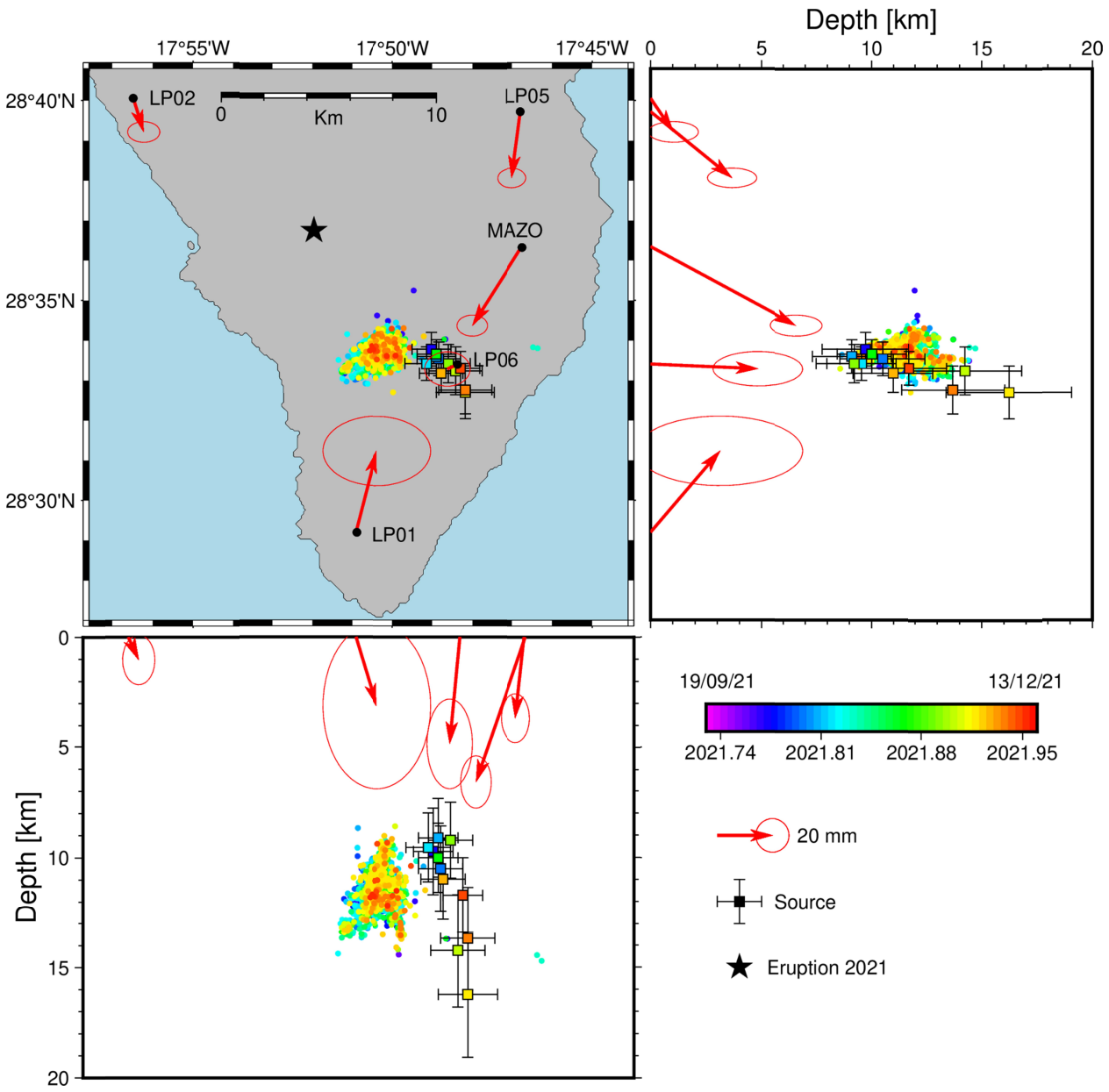

Figure 1. Active southern sector of La Palma Island (Cumbre Vieja volcano). Black star represents the 2021 eruption location. Black dots indicate the GNSS site locations (LP03 and LP04 are disregarded as explained at text) with displacements registered for the 85 days of eruption (red arrows). Deformation and seimicity sources are represented by the coloured squares and dots, respectively. Depth is shown for vertical cross-sections in N-S direction (top right panel) and E-W direction (bottom panel).

2.1. Ground deformation observations

Figures 1 and 2 show resulting continuous GNSS measurements at some network stations. Daily syn-eruptive GNSS time series (Figure 2) show a more or less radially inward pattern concordant with a regional subsidence at the island that began with the onset of Cumbre Vieja eruption on September 19, 2021. Whereas LPAL shows a southeastern displacement, LP05 and MAZO show a southwestern displacement and LP01 a northeastern one. All the stations show a vertical component of displacement which is more punctuated on LP06 station. Data from LP03 and LP04 continuous GNSS stations are strongly affected by local deformation caused by the large westerly dipping dike that fed the eruption (see e.g., De Luca et al., 2022; Fernández et al., 2022) and local changes in topography caused by lava flows. Therefore, we decided disregard data from LP03 and LP04 stations for the forecast and focuses on regional syn-eruptive subsidence registered by the stations furthest away from the eruption (LP01, LP02, LP05, LP06, MAZO and LPAL).

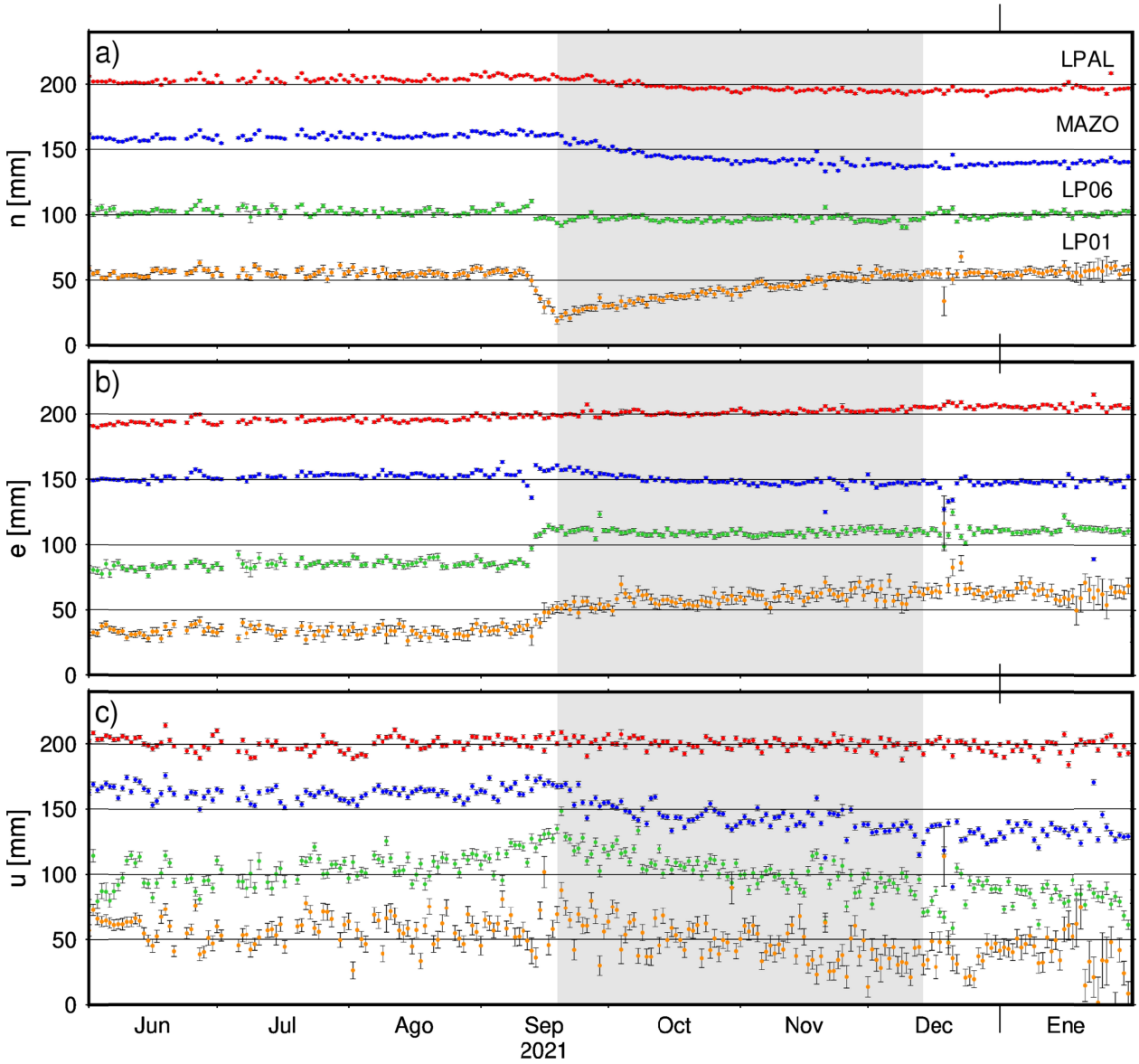

Figure 2. Daily GNSS time series. (a) North (n), (b) East (e) and (c) Vertical (u) component displacements at LPAL (red), MAZO (blue), LP06 (green) and LP01 (orange) GNSS stations. Gray shadow area corresponds to the eruption period in all figures.

2.2. Temporal changes on GNSS stations baseline lengths

We investigated the changes in length of different baselines of network configuration (Figure 3a) resulting from the ground contraction described above. Considering the distance and height differences of the ground where stations are installed, just horizontal displacements are considered to calculate temporal changes on baselines lengths. Changes in length resemble an exponential trend for all baselines formed taking LP01 as a reference station.

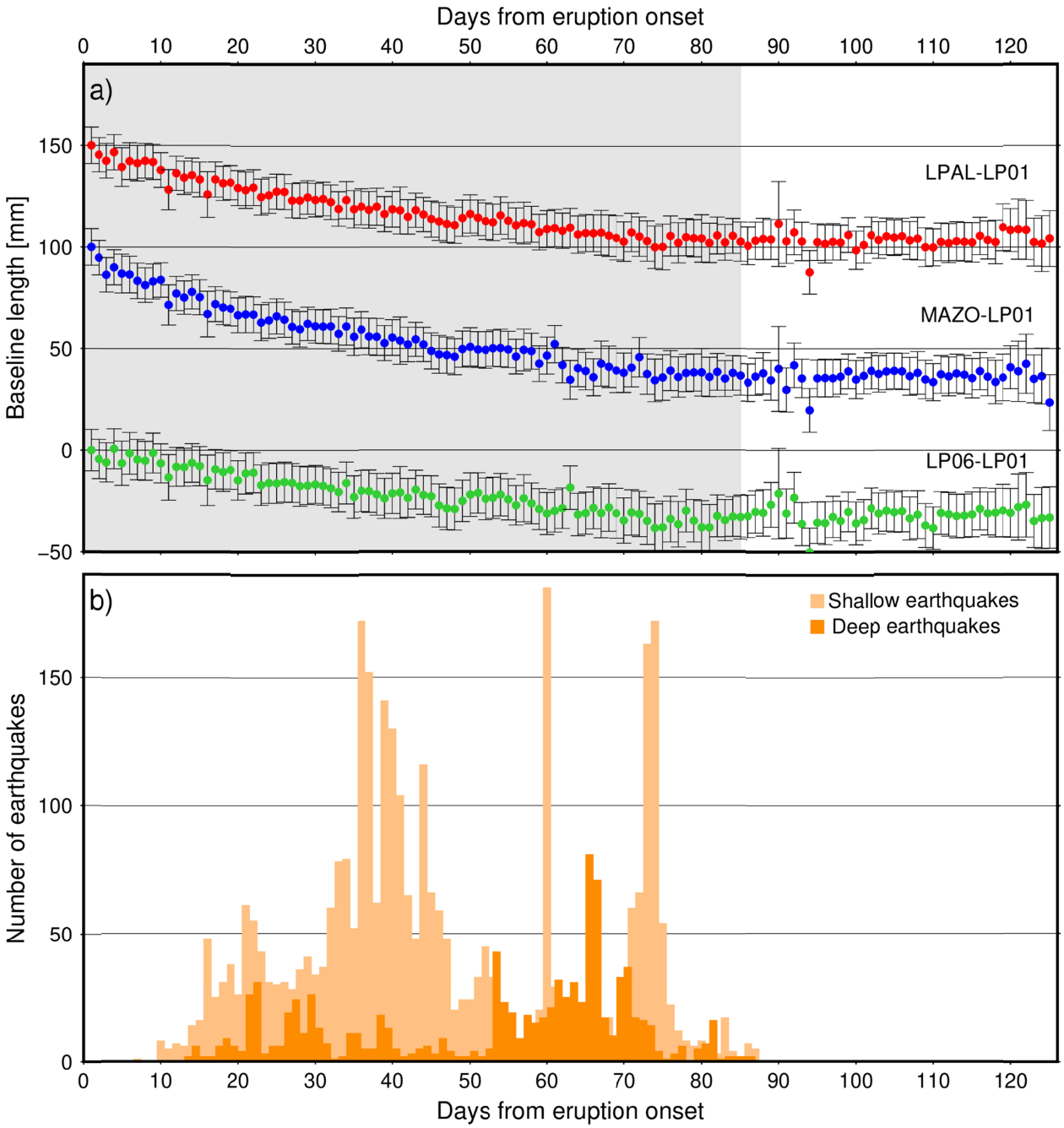

Figure 3. (a) *T*emporal change in baseline lengths since the eruption onset (day 0) calculated from LP01 station. LPAL-LP01, MAZO-LP01 and LP06-LP01 baselines changes are shown in red, blue and green, respectively. (b) Daily number of earthquakes since the eruption onset. Light orange corresponds to earthquakes at ~10-14 km depth whereas dark orange corresponds to seismicity at ~33-39 km depth.

2.3. Seismicity during the eruption

Seismicity was very weak and scarce during the first week of the eruption. However, a drastic change in seismicity occurred on 27 September and a dense and intense co-eruptive swarm started. Earthquakes were located under the central part of Cumbre Vieja and were distributed in two clusters at different depths. According to the relocation of Del Fresno et al. (2023), the first and most active cluster was located at ~10-14 km depth (Figure 1). The second cluster was located at ~33-39 km depth and its activity did not start until 5 October. This deeper cluster contained the largest earthquakes of the series (Local magnitude, ML>4.0). Seismic rates at both clusters varied considerably throughout the eruption showing maximum intensification peaks in November and December (Figure 3b).

3 Methods

3.1. Ground deformation magmatic source characterization

We analyze a possible temporal and spatial evolution of the source responsible for the observed syn-eruptive deflation by inverting cumulative daily deformation from the day that eruption started. We employ an analytical model of point pressure source (Mogi, 1958) because it is the simplest model that explains the signal within observation uncertainties. The horizontal location and depth of the source were computed using the MATLAB-based software package GBIS (Geodetic Bayesian Inversion Software, Bagnardi and Hooper, 2018). An elastic, homogeneous, isotropic half-space Poisson's ratio of 0.25 was assumed. GBIS estimates source parameters through a Markov Chain Monte Carlo simulation and uses dMODELS software package (Battaglia et al., 2013) for forward modeling.

3.2. Parametric exponential model for cumulative shortening

Temporal changes in length baseline curves show an exponential trend (Figure 3a) with gradually decreasing rates. We purpose a model of the form of equation (1) to estimate the overall temporal evolution of length changes due to deflation of the media. Thus, according to (1), time t_*, corresponding to a change in length threshold, $s_* = s(t_*)$ is given by:

$$t_* = -\tau ln(1 - s_*/s_o) \,, \qquad (2)$$

i.e., if early monitoring data during the eruption can be used to constrain the value of τ, an estimation of the time t_* at which the change in length rises the threshold, s_*, can be made. Here, s_* will correspond to syn-eruptive deflation stagnation and/or subsidence masked below the GNSS detection limit.

4 Results

4.1. Source characterization

The lack of substantial changes in the trends of GNSS time series (Figure2) indicates that the source responsible for regional subsidence might not have changed position during the eruption. We revisited this assumption of location stability by tracking movements of the source of deformation at different periods of time since the eruption onset. Some apparent movement of the source (Figure 1) is observed. This could reflect different regions of a magma reservoir being active at different times as seismicity mirror. However, due to data uncertainties, we assume that the deformation source remained stationary during the eruption being not possible confidently distinguished separate active regions.

191 The depth of the source is consistent with the upper bounds of the hypocentral depths (~ 10-14
192 km) of the seismic cluster active beneath the central area of Cumbre Vieja during the eruption
193 (Figure 1). Although the depths obtained for this cluster are slightly shallower for other authors (
194 ~7-11 km according to D'Auria et al. 2022), both depth ranges are consistent with Moho
195 discontinuity location at La Palma (see e.g., Banda et al., 1981; Ranero et al., 1995; Martínez-
196 Arevalo et al., 2013) where stagnation levels for ascending magmas at ephemeral reservoirs that
197 could last from decades to a few centuries are highly presumable (see e.g., González et al., 2013;
198 Klüegel et al., 2022; Ubide et al., 2022).

199 The estimated horizontal position of deformation source is approximately located in the middle
200 of the baseline between LP01 and MAZO stations, i.e., LP01 and MAZO would be able to
201 register horizontal displacements of maximum absolute magnitude according to Mogi model.
202 Therefore, LP01-MAZO baseline is excellent to study the syn-eruption subsidence.

203 **4.2. Time series of cumulative shortening**

204 We estimate the end of ground deflation by using LP01-MAZO baseline and the model (1).
205 Initially, when we started to analyzed length changes, we employed the available GNSS dataset,
206 that spans 38 days after the day that eruption started, for constraining the value of τ.

207 Figure 4 shows the extrapolation of the best-fit exponential curves given by (1) based on some
208 datasets since the eruption onset (Models A, B1 and B2). Some discrepancies are observed
209 between the data and the best fit curve estimated from 38 days of data (Model A). Nevertheless,
210 the stabilization on the trend of the daily estimations of t_* (Figure 5) pointed out that the
211 estimated e-folding time-scale, $\tau = 18.6$ days, was good enough to forecast a range for the
212 stagnation of subsidence signals. We forecasted a continuous deflation, at diminishing rates,

lasting $t_* \in [56, 86]$ days (Table S1 and Figure 5a). Following equation (2), the interval bounds correspond to some detection limits on horizontal displacements that are going to be dictated by a change in length between the 5% and 1% of the change in length that could have been registered before the eruption onset, $(1 - s_*/s_o)$.

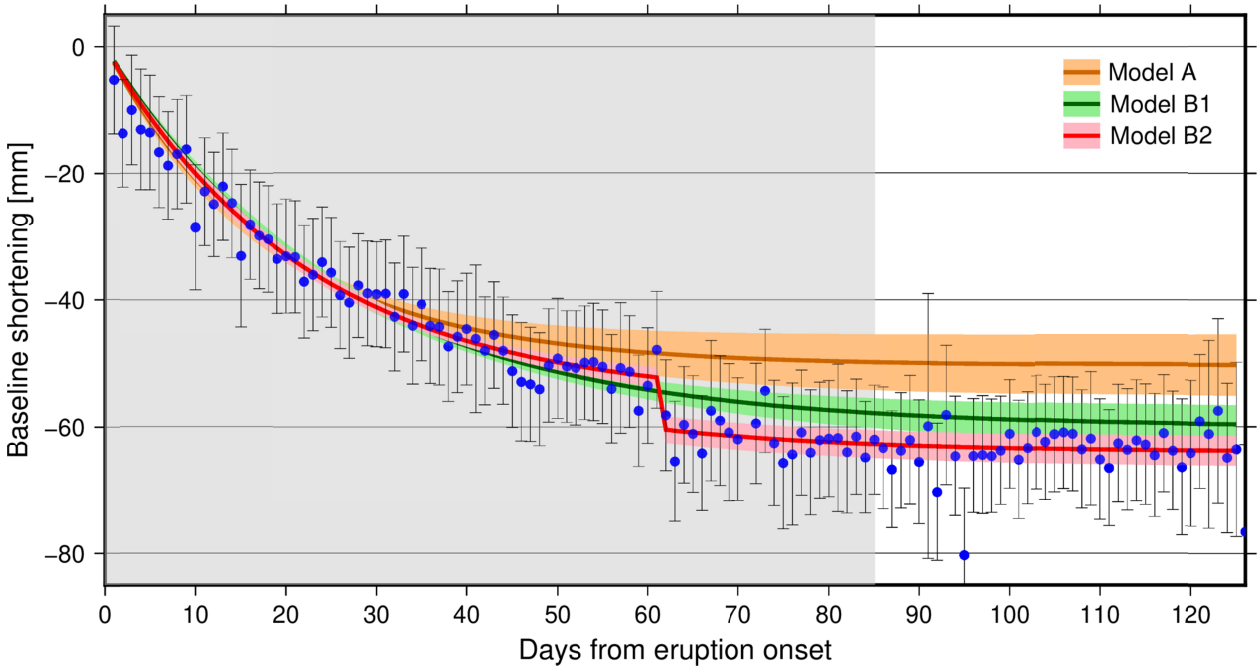

Figure 4. Extrapolation of the best-fit curves (dark color lines) based on cumulative shortening of baseline MAZO-LP01 (blue dots and error bars) from day 1 of eruption. Light color shadows correspond to the 95% uncertainty bounds of each model. Orange: Model A obtained from data of 38 days since eruption onset; green: Model B1 the same considering 70 days and red: Model B2 same as Model B1 considering an acceleration of the subsidence on day 62 (offset).

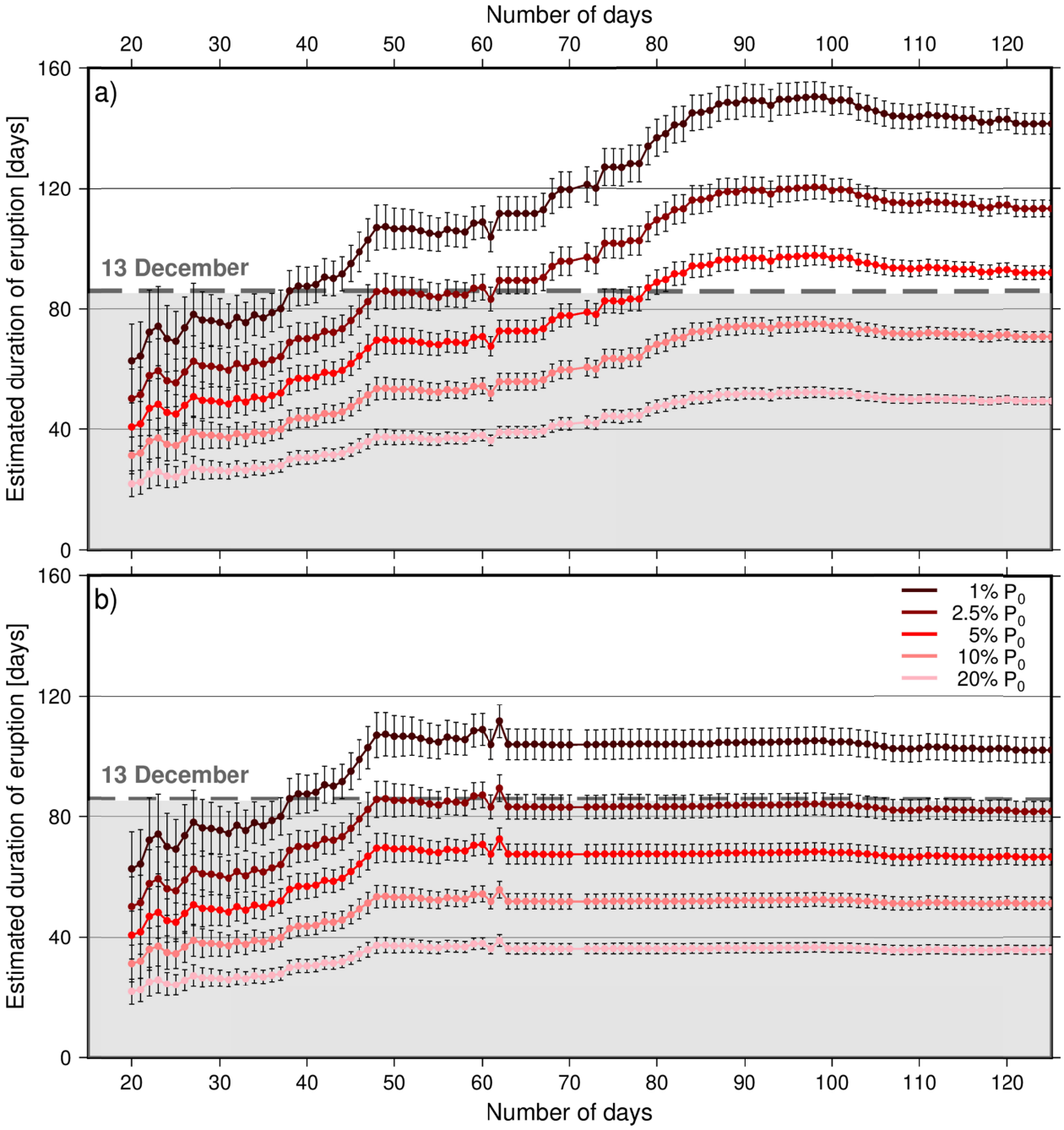

Figure 5. Daily estimations of t_* since the day 20 from the eruption onset. We consider different scenarios for the eruption end based on pressure drop (ΔP^*) thresholds that are reached as a fraction (20, 10, 5, 2.5 and 1%) of the reservoir overpressure when the eruption started (P_0).

5. Discussion

5.1. Pressure drop as forecasting tool for the end of the eruption

The 2021 eruption of Cumbre Vieja is the best instrumentally recorded to date at Canary Islands. Estimates of SO2 injected mass into the atmosphere and ash depositions during the eruption (Milford et al., 2023) decay monotonically in parallel with our changes in baseline length evolution. Specifically, the observed change in baseline length follows equation (1) and therefore this change should asymptotically approach a final, constant value.

Within the elastic assumption of media, deflation (or any displacement measurement) is proportional to reservoir decompression , i.e., the observed changes in length, $s(t)$, are proportional to a pressure drop (ΔP) that physically could be related to fluid depressurization due to magma withdrawal and/or migration in a reservoir (see e.g., Stasiuk et al., 1993; Huppert and Woods, 2002; Mastin et al., 2009; Anderson and Segall, 2011). Considering the magma plumbing system of the island as a closed system where syn-eruptive, quasi-instantaneous subsidence is expected in response to the removal of magma and gas during the eruption (see e.g., Chaussard et al., 2013), we defined a threshold on pressure drop, ΔP^* as the pressure drop needed for eruption coming to its end. ΔP^* was given as a function of some fractions of the overpressure of the reservoir needed to promote an eruption or an intrusion (P_0) since, a priori, we did not know the values at which those pressure changes were balanced during the eruption. Therefore, we used the model (1) to project the eruption's final duration given that the relationship between ΔP and P_0 is proportional to the e-folding time, $\tau = 18.6$ days. The forecast performed during the eruption for deflation end fell between $[56, 86]$ days. Thus, ΔP^* fell between $[56, 86]$ days in absence of new magma recharges or volatiles exsolution. These limits correspond to a 5% and 1% fraction of P_0 respectively (Table S1; Figure 5a). The

eruption ended on December, 13, i.e., the eruption end was consistent with a pressure drop of $\Delta \boldsymbol{P}^* = \mathbf{0.01}\boldsymbol{P_0}$.

Historical records of the duration of La Palma eruptions are between 24 and 84 days (e.g., Romero, 1990). Our model, under simple assumptions and thanks to the good permanent GNSS network, provides an estimate of duration of 86 days with a forecasting uncertainty window of $[79.3, 92.7]$ days for $\Delta \boldsymbol{P}^* = \mathbf{0.01}\boldsymbol{P_0}$ (Table S1). Therefore, almost halfway along the duration of the eruption, and even gas levels or other parameters did not point yet to the end of the eruption (e.g., El Español, 27/10/2021), the proposed model could help to point out that the estimated duration resembles the longest duration of historical eruptions in La Palma.

5.2. Hindcast: validation of the tool for forecasting

Real-time updates on the estimations of the characteristic e-folding time, duration and cessation of the eruption can be made using daily GNSS time series data. Here, we perform a post-eruption analysis given daily hindcast updates. Unsurprisingly, we observe that the accuracy of the estimations increases with the number of data points, therefore the end of the eruption forecast can be improved including new temporal data.

Figure 5 shows the best-fit values of eruption duration as a function of the portion of initial overpressure that remains in the reservoir (P_0) versus the day of hindcast. During the first 5 to 20 days of eruption the fitting of the model (1) is poor since we do not have enough data to accurately confirm an exponential trend. Therefore, the hindcast is too poor and it is not shown. The estimations on the duration of the eruption, although the trend is mainly stable, present some offsets and seem to increase with the number of data that feed the model parametrization (Figure 5a). A recharge pulse might increase the estimations of duration of the eruption with time.

However, we would expect in response a geodetic re-inflation signal whereas we observe a continued deflation at GNSS time series (Figures 2 and 3) that produces a downward-propagating relaxation as proposed for the forecast (Figure 4). Furthermore, changes in length data are within the 95% credible bounds calculated for the extrapolation of the best-fit curve employed for forecast (Figure 4, Model A). In hindcast, we observe that these bounds are narrowed as the number of days increases (Figure 4, Model B1). All these results would seem to argue in favor of the model proposed for the cumulative change of baseline lengths to estimate the end of the eruption.

The extrapolation of the best-fit model posed a divergence with data around the 58-65 day that could not be explained by data uncertainty (Figure 4; Model A). A model that comprises around 70 days can account for the observed divergence although provides a poorer fit for the initial days of eruption (Figure 4; Model B1). During the divergence period, an acceleration on the rate of change in length is observed (Figure 3 and 4).

We propose adding an offset to model (1) on day 62 to estimate such acceleration (Figure 4; Model B2). Such a model presents a very good fit and can account for the observed changes in length. Furthermore, a stable hindcast is obtained considering data from the day around 47-48 of eruption (Figure 5b). We note that, in hindcast, the most stable and accurate forecast was achieved with a $\Delta \boldsymbol{P}^{*} = \mathbf{0.025}\boldsymbol{P_0}$ condition.

The proposed offset on length changes temporally correlates with the opening of an unexpected fissures and vents system during the eruption's last phase (González, 2022), the peak of shallow seismicity registered at ~10-14 km depth, an increase of the number of earthquakes registered at ~33-39 km depth (Figure 3b) and it is anticorrelated with peaks of high daily effusion rates

observed using satellite observations (Plank et al., 2023). Future work should include detailed investigations on such correlations in order to increment the success and accuracy of the proposed forecasting tool. The geophysical relevance of the specific value achieved for ΔP^* should be investigated too, and compared across similar eruptive processes.

6. Conclusions

During the 2021 La Palma eruption, it was possible to generate an accurate forecast for the end of the eruption. Nevertheless, the forecast was not significantly relevant in operational terms due to the large uncertainty on the estimations of the threshold of pressure drop needed to the eruption coming to an end that was given by some fractions of the overpressure needed to drive the eruption. Such forecasting exercise was possible given the configuration of the GNSS permanent stations and assuming pressure drop follows the asymptotic flattening of the exponential changes in length of GNSS baselines. Under similar conditions (an exponential decay), an actionable (under emergency managing circumstances) and credible forecast would be possible after the time-scale around e-folding time. Based on the hindcast analysis, more accurate forecasts could be obtained from the time-scale of 2τ. This approach relies on a chamber undergoing a release of elastic energy during an eruption. Considering this framework, net magma withdrawal to feed the eruption seems to be dominated by the dynamics of a Moho depth reservoir beneath Cumbre Vieja volcano.

Acknowledgments and data Availability Statement

We thank Mike Poland (USGS) for the prompt feedback on the preliminary methodology during the course of the volcanic crisis. We also thank the IGN team for supporting the installation and maintenance of the volcano monitoring stations. We thank Spanish Research Agency projects PID2019-104571RA-I00 funded by MCIN/AEI/10.13039/501100011033 and PID2020-114682RB-C32 funded by AEI / 10.13039/501100011033. Research activities of the CSIC staff during the eruption were funded by CSIC through the CSIC-PIE project with ID number PIE20223PAL008 (Real Decreto 1078/2021, de 7 de diciembre). This work was also partially supported by project PTDC/CTA-GEO/2083/2021 GEMMA, funded by Fundação para a Ciência e a Tecnologia (FCT) I.P./MCTES. Figures were obtained using Generic Mapping Tools (GMT) (Wessel, P., Luis, J. F., Uieda, L., Scharroo, R., Wobbe, F., Smith, W. H. F., & Tian, D. (2019). The Generic Mapping Tools version 6. *Geochemistry, Geophysics, Geosystems*, 20, 5556–5564. https://doi.org/10.1029/2019GC008515). Data from LP01 and MAZO GNSS stations used for the forecast and pressure drop that support the work (cumulative changes in length) are open access from Instituto Geográfico Nacional (https://www.ign.es/web/gds-gnss-datos-rinex) and GRAFCAN (https://gnss.grafcan.es).

References

Altamimi, Z., Rebischung, P., Métivier, L. & Collilieux, X. (2016), ITRF2014: A new release of the International Terrestrial Reference Frame modeling nonlinear station motions. J. Geophys. Res. Solid Earth 121 88), 6109-6131, https://doi.org/10.1002/2016JB013098

Anderson, K., and Segall, P. (2011), Physics-based models of ground deformation and extrusion rate at effusively erupting volcanoes. J. Geophys. Res., Solid Earth 116(B7), B07204, https://doi.org/10.1029/2010JB007939

Banda, E., J. J. Dañobeitia, E. Surinach, and J. Ansorge (1981), Features of crustal structure under the Canary Islands, Earth Planet. Sci. Lett., 55, 11–24, doi:10.1016/0012-821X(81)90082-0.

Bagnardi, M., and Hooper, A. (2018), Inversion of surface deformation data for rapid estimates of source parameters and uncertainties: a bayesian approach. *G-cubed* 19, 2194–2211. doi:10.1029/2018GC007585.

Battaglia, M., Cervelli, P., and Murray, J. (2013), DMODELS: a MATLAB software package for modeling crustal deformation near active faults and volcanic centers. *J. Volcanol. Geoth. Res.* 254, 1–4. doi:10.1016/j.jvolgeores.2012.12.018.

Biggs, J., and Pritchard, M. E. (2017). Global volcano monitoring: whatdoes it mean when volcanoes deform? Elements, 13(1), 17-22.https://doi.org/10.2113/gselements.13.1.17

Coppola, D., Ripepe, M., Laiolo, M., and Cigolini, C. (2017). Modelling satellite-derived magma discharge to explain caldera collapse. Geology, 45 (6), pp. 523-526, https://doi.org/10.1130/G38866.1

Chaussard, E., Amelung, F. and Aoki, Y. (2013), Characterization of open and closed volcanic systems in Indonesia and Mexico using InSAR time series. J. Geophys. Res.: Solid Earth, 118 (8), 3957-3969, https://doi.org/10.1002/jgrb.50288

363 Coppola, D., Ripepe, M., Laiolo, M., Cigolini, C. (2017). Modelling satellite-derived magma
364 discharge to explain caldera collapse. *Geology* 2017;; 45 (6): 523–526. doi:
365 https://doi.org/10.1130/G38866.1
366
367 Dach, R., Lutz, S., Walser, P., Fridez, P. (2015), Bernese GNSS Software Version 5.2.
368 doi:10.7892/boris.72297.
369
370 D'Auria, L., Koulakov, I., Cabrera-Perez, I., *et al.* (2022). Voluminous Storage and Rapid
371 Magma Ascent Beneath La Palma Revealed by Seismic Tomography. *Sci. Rep.*, 1–14.
372 https://doi.org/10.1038/s41598-022-21818-9
373 De Luca, C., Valerio, E., Guidicipietro, F., Macedonio, G., Casu, F., Lanari, R. (2022), Pre- and
374 co-eruptive analysis of the September 2021 eruption at Cumbre Vieja volcano (La Palma, Canary
375 Islands) through DInSAR measurements and analytical modeling. *Geophys. Res. Lett.*, 49 (7),
376 e2021GL097293, https://doi.org/10.1029/2021GL097293
377
378 Dvorak, J.J. and Okamura, A.T. (1987). A hydraulic model to explain variations in summit tilt
379 rate at Kilauea and Mauna Loa Volcanoes, R.W. Decker, T.L. Wright, P.H. Stauffer (Eds.),
380 Volcanism in Hawaii, vol. 2, *U. S. Geol. Surv. Prof. Pap.*, vol. 1350 (1987), pp. 1281-1296.
381
382 Del Fresno, C., Cesca, S., Klügel, A. *et al.* (2023) Magmatic plumbing and dynamic evolution of
383 the 2021 La Palma eruption. *Nat Commun* **14**, 358. https://doi.org/10.1038/s41467-023-35953-y
384
385 El Español (2021) "Así se apagará el volcán de La Palma: las tres señales que avisan del final de
386 una erupción", 27/10/2021, https://www.elespanol.com/ciencia/medio-
387 ambiente/20211027/apagara-volcan-palma-senales-avisan-final-erupcion/622438480_0.html
388
389 Fernández, J., Escayo, J., Camacho, A.G. *et al.* Shallow magmatic intrusion evolution below La
390 Palma before and during the 2021 eruption. *Sci Rep* **12**, 20257 (2022).
391 https://doi.org/10.1038/s41598-022-23998-w
392

González P.J., Samsonov S., Pepe S., *et al.* (2013), Magma storage and migration associated with the 2011-2012 El Hierro eruption: Implications for shallow magmatic systems at oceanic island volcanoes, *J. Geophys. Res. – Solid Earth*, 118, 4361–4377, doi:10.1002/jgrb.50289

González, P.J. (2022), Volcano-tectonic control of Cumbre Vieja. *Science*, **375**, 1348–1349, DOI: 10.1126/science.abn51.

Gudmundsson, M.T., Jonsdottir, K., Hooper, A., Holohan, E.P., Halldorsson, S.A., Ofeigsson, B.G., Cesca, S., Vogfjord, K.S., Sigmundsson, F., Hognadottir, T., Einarsson, P., Sigmarsson, O., Jarosch, A.H., Jonasson, K., Magnusson, E., Hreinsdottir, S., Bagnardi, M., Parks, M.M., Hjorleifsdottir, V., Palsson, F., Walter, T.R., Schopfer, M.P.J., Heimann, S., Reynolds, H.I., Dumont, S., Bali, E., Gudfinnsson, G.H., Dahm, T., Roberts, M.J., Hensch, M., Belart, J.M.C., Spaans, K., Jakobsson, S., Gudmundsson, G.B., Fridriksdottir, H.M., Drouin, V., Durig, T., Adalgeirsdottir, G., Riishuus, M.S., Pedersen, G.B.M, van Boeckel, T., Oddsson, B., Pfeffer, M.A., Barsotti, S., Bergsson, B., Donovan, A., Burton, M.R., and Aiuppa, A. (2016). Gradual caldera collapse at Bardarbunga volcano, Iceland, regulated by lateral magma outflow. *Science*, 353 (6296) (2016), p. 262, DOI:10.1126/science.aaf8988

Hreinsdóttir, S., Sigmundsson, F., Roberts, M. *et al.* (2014), Volcanic plume height correlated with magma-pressure change at Grímsvötn Volcano, Iceland. *Nature Geosci* **7**, 214–218. https://doi.org/10.1038/ngeo2044

Huppert, H.E., Woods, A.W. (2002). The role of volatiles in magma chamber dynamics. Nature 420 (6915), 493-495, https://doi.org/10.1038/nature01211

Kouba, J. (2009), A guide to using international GNSS service (IGS) products. International GNSS Service.

Klügel A, Albers E, Hansteen, TH (2022): Mantle and crustal xenoliths in a tephriphonolite from La Palma (Canary Islands): implications for phonolite formation at oceanic island volcanoes. *Frontiers in Earth Science - Volcanology* 10:761902.

Lengliné, O., Marsan, D., Got, J.L., Pinel, V., Ferrazzini, V. and Okubo, P.G (2008). Seismicity and deformation induced by magma accumulation at three basaltic volcanoes, J. Geophys. Res., 113 (2008), Article B12305, 10.1029/2008JB005937

Lyard, F., Lefevre, F., Letellier, T. & Francis, O. (2006), Modelling the global ocean tides: modern insights from FES2004. Ocean Dyn. 394–415, https://doi.org/10.1007/s10236-006-0086-x.

Machado, F. (1974), The search for magmatic reservoirs. *In* Civetta, L., et al. eds., Physical Volcanology: Amsterdam, Elsevier, Developments in Solid Earth Geophysics, v. 6, p. 255–273, doi:10.1016/B978-0-444-41141-9.50017-6.

Martinez-Arevalo, C., de Lis Mancilla, F., Helffrich, G. & Garcia, A., (2013), Seismic evidence of a regional sublithospheric low velocity layer beneath the Canary Islands. Tectonophysics 608, 586–599, https://doi.org/10.1016/j.tecto.2013.08.021.

Marzocchi, W. and Bebbington, M.S. (2012), Probabilistic eruption forecasting at short and long time scales. *Bull Volcanol* **74**, 1777–1805. https://doi.org/10.1007/s00445-012-0633-x

Mastin, L.G., Lisowski, M., Roeloffs, E., and Beeler, N. (2009), Improved constraints on the estimated size and volatile content of Mount St. Helens magma system from the 2004-2008 history of dome growth and deformation. Geophys. Res. Lett., 36, https://doi.org/10.1029/2009GL039863.

Milford, C., Torres, C., Vilches, J., Gossman, A-K., Weis, F., Suárez-Molina, D., García, O.E., Prats, N., Barreto, A., García, R.D., Bustos, J.J., Marrero, C.L., Ramos, R., Chinea, N., Boulesteix, T., Taquet, N., Rodríguez, S., López-Darias, J., Sicard, M., Córdoba-Jabonero, C., Cuevas, E., (2023) Impact of the 2021 La Palma volcanic eruption on air quality: Insights from a multidisciplinary approach, Science of The Total Environment, Volume 869, 161652, https://doi.org/10.1016/j.scitotenv.2023.161652.

454 Mogi, K. (1958). Relations between the eruptions of various volcanoes and the deformations of
455 the ground surfaces around them. *Bull. Earthquake Res. Inst. Univ. Tokyo.* 36, 99–134.
456
457 National Academies of Sciences, Engineering and Medicine (2017). Volcanic eruptions and their
458 repose, unrest, precursors, and Timing (p. 134). Washington, DC: The National Academies
459 Press. https:// doi.org/10.17226/24650.
460
461 Pallister, J. and McNutt, S.R. (2015). Synthesis of Volcano Monitoring. in H. Sigurdsson (Ed.),
462 *The Encyclopedia of Volcanoes (2nd Ed.)*, Academic Press, p. 1151-1171,
463 https://doi.org/10.1016/B978-0-12-385938-9.00066-3.
464
465 Plank, S., Shevchenko, A.V., d'Angelo, P. *et al.* Combining thermal, tri-stereo optical and bi-
466 static InSAR satellite imagery for lava volume estimates: the 2021 Cumbre Vieja eruption, La
467 Palma. *Sci Rep* **13**, 2057 (2023). https://doi.org/10.1038/s41598-023-29061-6
468
469 Poland, M. and Anderson, K. (2019), Partly cloudy with a chance of Lava flows: Forecasting
470 volcanic eruptions in the Twenty-First Century. J. Geophys. Res.: Solid Earth, 125,
471 e2018JB016974, https://doi.org/10.1029/2018JB016974.
472
473 Ranero, C.R., Torne, M. & Banda, E. Gravity and multichannel seismic reflection constraints on
474 the lithospheric structure of the Canary Swell. *Mar Geophys Res* **17**, 519–534 (1995).
475 https://doi.org/10.1007/BF01204342
476
477 Romero, C. (1990), Las manifestaciones volcánicas históricas del Archipiélago Canario. PhD
478 Thesis, 791 pp. https://riull.ull.es/xmlui/handle/915/10113.
479
480 Rodríguez-Molina, S., González P.J., Charco, M., Negredo, A.M., Schmidt, D.A., (2021) Time-
481 Scales of inter-eruptive Volcano Uplift Signals: Three Sisters Volcanic center, Oregon (USA).
482 Frontiers in Earth Science, 8(645), 1-30, doi:10.3389/feart.2020.577588
483

484 Segall, P. (2013), Volcano deformation and eruption forecasting, Remote Sensing of Volcanoes
485 and Volcanic Processes: Integrating Observation and Modelling, D. M. Pyle, T. A. Mather, J.
486 Biggs. Ed.: Geol. Soc. London, 29p., https://doi.org/10.1144/SP380.4
487
488 Sparks, R.S.J. (2003), Forecasting volcanic eruptions. Earth Planet. Sci. Lett., 210(1-2), 1-15,
489 https://doi.org/10.1016/S0012-821X(03)00124-9.
490
491 Stasiuk, M.V., Jaupart, C., and Sparks, R.S.J. (1993), On the variations of flow-rate in
492 nonexplosive lava eruptions. Earth Planet. Sci. Lett. 114(4), 505-516,
493 https://doi.org/10.1016/0012-821X(93)90079-O.
494
495 Ubide, T., Larrea, P., Becerril, L. and Galé; C. (2022); Volcanic plumbing filters on ocean-island
496 basalt geochemistry. *Geology*; 50 (1): 26–31. doi: https://doi.org/10.1130/G49224.1
497
498 Wadge, G. (1981), The variation of magma discharge during basaltic eruptions. J. Volcanol.
499 Geotherm. Res., 11, 139–168, doi:10.1016/0377-0273(81)90020-2.